Volume 12 Number 1 7 January 2016 Pages 1–314

Soft Matter

www.softmatter.org

ISSN 1744-683X

ROYAL SOCIETY OF CHEMISTRY

PAPER
Jure Dobnikar et al.
Rational design of molecularly imprinted polymers

175 YEARS

This is an Accepted Manuscript, which has been through the Royal Society of Chemistry peer review process and has been accepted for publication.

Accepted Manuscripts are published online shortly after acceptance, before technical editing, formatting and proof reading. Using this free service, authors can make their results available to the community, in citable form, before we publish the edited article. We will replace this Accepted Manuscript with the edited and formatted Advance Article as soon as it is available.

You can find more information about Accepted Manuscripts in the author guidelines.

Please note that technical editing may introduce minor changes to the text and/or graphics, which may alter content. The journal's standard Terms & Conditions and the ethical guidelines, outlined in our author and reviewer resource centre, still apply. In no event shall the Royal Society of Chemistry be held responsible for any errors or omissions in this Accepted Manuscript or any consequences arising from the use of any information it contains.

The Dynamics of Rising Oil-Coated Bubbles: Experiments and Simulations

Songcheng Wang[†], Yi Zhang[†], J. Carson Meredith[†], Sven H.
Behrens[†*], Manoj Kumar Tripathi[††] and Kirti Chandra Sahu[†††*]
[†]*School of Chemical & Biomolecular Engineering,
Georgia Institute of Technology, Atlanta,
Georgia 30332-0100, United States*
[††]*Department of Chemical Engineering,
Indian Institute of Science Education and Research Bhopal 462 066,
Madhya Pradesh, India*
[†††]*Department of Chemical Engineering,
Indian Institute of Technology Hyderabad,
Kandi, Sangareddy 502 285, Telangana, India*

(Dated: February 17, 2018)

Air bubbles rising through an aqueous medium have been studied extensively and are routinely used for the separation of particulates via froth flotation, a key step in many industrial processes. Oil-coated bubbles can be more effective for separating hydrophilic particles with low affinity for the air-water interface, but the rise dynamics of oil-coated bubbles has not yet been explored. In the present work, we report the first systematic study of the shape and rise trajectory of bubbles engulfed in a layer of oil. Results from direct observation of the coated bubbles with a high-speed camera are compared to computer simulations and confirm a pronounced effect of the oil coat on the bubble dynamics. We consistently find that the oil-coated bubbles display a more spherical shape and straighter trajectory, yet slower rise than uncoated bubbles of comparable size. These characteristics may provide practical benefits for flotation separations with oil-coated bubbles.

Significance:

The familiar phenomenon of air bubbles rising in water can not only be mesmerizing to watch; it also has many important industrial applications, where bubble flotation is routinely used to extract solid particles from a liquid medium. Some well-known limitations of this separation method can be overcome by using bubbles coated with a layer of oil. What the presence of such an oil coat means for the otherwise well-known bubble dynamics, however, has not yet been explored. Our present experimental and computational study compares oil-coated and uncoated bubbles with similar size and buoyancy rising through water. Observed systematic differences in the trajectory, shape, and rise velocity are significant both for industrial operations and for our fundamental understanding of bubble dynamics.

I. INTRODUCTION

Froth flotation, a highly efficient separation method, has been widely utilized in many industrial processes, including mineral separations [1–3], bitumen recovery [4–6], deinking processing [7–9] and waste water treatment [10–12], to name a few. The basic principle in this method is that solvophobic particles will attach to gas bubbles and will be lifted to the surface as the bubbles rise due to buoyant forces, whereas more solvophilic components will remain in the liquid. For particle removal from aqueous dispersions or slurries by air flotation, the particles need to be either naturally hydrophobic or need to be rendered as hydrophobic by surface treatments. Some reagents, called collectors, can selectively adsorb onto the particle surface and tune the hydrophobicity of the particles [13]. However, this may sometimes cause undesired synergistic interactions among collectors, activators, depressants and dispersants in the slurry. The use of collectors also tends to decrease the separation selectivity and increases costs [14, 15].

Many efforts have been made to avoid or minimize the use of collectors. One such alternative is to tune the hydrophobicity of the air bubbles, not the particles. As early as 1927, Taggart [16] suggested that an oil film formed outside the air bubble can enhance the flotation performance. By coating the air bubble with a thin film of oil, the bubble surface can be adjusted to be less hydrophobic (compared to uncoated bubble) to allow adsorption of less hydrophobic or even mildly hydrophilic particles. This idea of oil-coated bubbles has been applied in many areas. Liu *et al.* [15] covered air bubbles with a thin layer of kerosene (containing a small amount of oil-soluble collectors) and developed the concept of reactive oily-bubble flotation. Zhou and co workers [17–19] studied the application of reactive

---

* sven.behrens@chbe.gatech.edu, ksahu@iith.ac.in

Soft Matter Accepted Manuscript

oily bubbles in bastnaesite flotation. Wallwork *et al.* [20] and Su *et al.* [21] applied "reactive oily bubbles" to bitumen recovery. Chen *et al.* [22] and Tarkan *et al.* [23] investigated the solvent extraction process using solvent-coated bubbles. Maiolo and Pelton [24] found that air bubbles coated with silicone oil can enhance deinking performance, and Gomez *et al.* [25] further investigated an aerosol-enhanced deinking process using oil-coated bubbles.

Since flotation performance is closely related to the dynamic rise behavior of air bubbles, it is of great interest to understand and predict bubble rise dynamics. The motion of uncoated bubbles has already been studied extensively by several researchers (see e.g, [26–30]). The shape deformation, breakup, and path instability have been investigated throughly. Recently, we have successfully used the volume-of-fluid (VOF) method with dynamic adaptive grid refinement to simulate the rise dynamics of an initially spherical air bubble rising from a quiescent liquid [31], and then applied the model to predict dynamics under several different flow conditions [32–34]. Tripathi *et al.* [31] also have identified five different regimes of starkly distinct behaviours (namely, axisymmetric, skirted, zigzagging/spiralling, peripheral break-up and central breakup regions of an air bubble rising in water). The dynamics of oil-coated air bubbles, by contrast, is still not well understood. As we shall see, the presence of an oil coat affects the overall bubble shape, velocity and trajectory, which in turn has consequences for the bubble-particle interaction in the flotation process.

To our knowledge, this paper presents the first systematic study of the dynamics of rising oil-coated bubbles. We generated oil-coated air bubbles without the help of surfactants or collectors, and measured their size, shape, trajectory, and rise velocity; the results were compared with those of uncoated bubbles. We further simulated the rise dynamics of oil-coated bubbles and compared the findings to our experimental data.

II. METHODS

The dynamics of an oil coated bubble rising in a liquid is investigated by conducting experiments and direct numerical simulations. The experimental set-up, the method used to post-process the data obtained using the high-speed imagining and numerical method used in order to simulate the rise dynamics of an oil-coated bubble are discussed below.

A. Experimental Procedure

1. Apparatus

The bubble rise experiments were carried out in a square Plexiglas column with dimensions of 15 cm × 15 cm × 100 cm. The schematic diagram of the set-up is shown in Figure 1. The column was filled with deionized water or other testing liquids to a depth of 80 cm. Bubbles were generated at the bottom of the column by using an apparatus described below. The bubble motion was recorded by a high-speed camera (Phantom v7.0, Vision Research, Inc.) and image acquisition software (PCC v2.8, Vision Research, Inc.). The illumination of the test region was provided by a lamp with a diffuser behind the rectangular column. A scale bar was immersed into the column to determine the size and position of the bubbles. Obtained image frames were then analyzed using the Image J software.

2. Materials

Silicone oil (10 cSt), and octane were purchased from Sigma-Aldrich and 1,6-Hexanediol diacrylate (HDDA) was obtained from Allnex Resins Co, Ltd. Octane and HDDA were purified with silica gel to remove any possible impurities. They were used to form oil-coated air bubbles. 2-hydroxy-2-methylopropiophenone was purchased from Sigma-Aldrich as the photo-initiator for the polymerization of HDDA. Ultra-pure water (18.2 MΩ-cm) was used as the medium fluid for observing bubble rise. Food grade cane sugar ("Great Value", Walmart) was used to adjust the medium fluid viscosity. The sugar solutions behave as Newtonian fluids for all the concentrations used in the present study. The purity of the sugar solutions was confirmed by measuring its surface tension and comparing it with literature values [35, 36].

3. Generating Oil-Coated Bubbles

Oils with positive spreading coefficient can completely engulf air bubbles [37]. Based on the material properties displayed in Table I, we chose the fully engulfing silicone oil, octane, and HDDA to form a stable film around the air
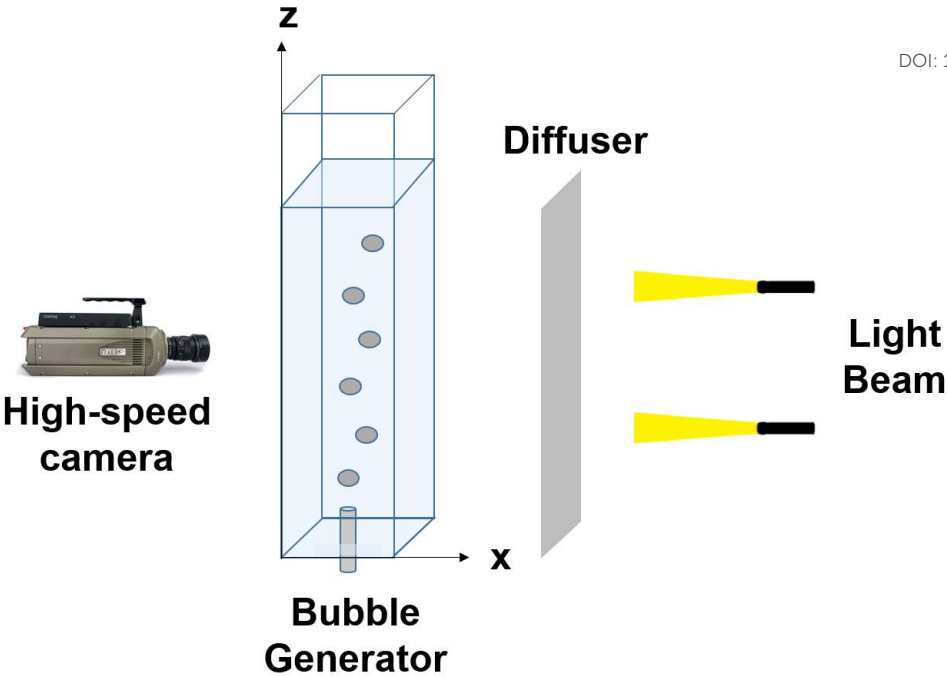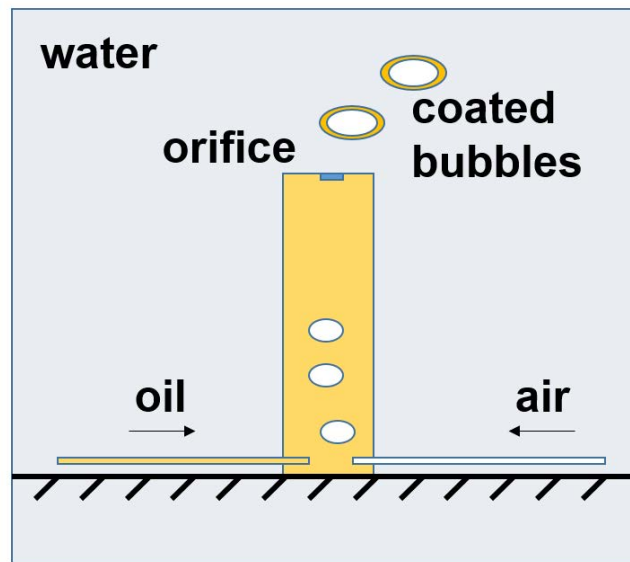
3

FIG. 1: Schematic diagram of the experiment apparatus.

bubbles. Coated bubbles can be generated in many ways. In our work, we designed a small polystyrene chamber with an orifice at the top as shown in Figure 2. The chamber was first filled with oil, then air was introduced slowly. Once a small air bubble penetrates the orifice, it exits into the water with an oil coating. Air and oil were dispensed using two syringe pumps (NE-300, New Era Pump Systems, Inc.).

TABLE I: Fluids properties of the fluids used. Here, all the interfacial tensions are equilibrium tension (i.e. both phases are mutually saturated before measurement). The interfacial tensions for silicone oil-40% (w.t.) sugar solution and octane-40% (w.t.) sugar solution cannot be measured with pendant drop method because the refractive index of both phases are too close to be distinguished.

Fluids	Density (g/cm^3)	Viscosity (cP)	Oil-air surface tension (mN/m)	Water-air surface tension (mN/m)	Oil-water interfacial tension (mN/m)	Spreading coefficient S_o (mN/m)
Saturated with DI water						
Silicone oil	0.93	9.3	18.8	69.3	41.3	9.2
Octane	0.7	0.5	21.2	72.8	43.9	7.7
HDDA	1.01	9.0	25.8	46.8	17.0	4.0
Saturated with 40% (w.t.) sugar solution (5.8 cP)						
Silicone oil	0.93	9.3	19.4	75.0	−	−
Octane	0.7	0.5	21.4	72.4	−	−
HDDA	1.01	9.0	32	49.7	16.4	1.3
Saturated with 50% (w.t.) sugar solution (13.0 cP)						
Silicone oil	0.93	9.3	21.5	75.3	39.9	13.9
Octane	0.7	0.5	20.7	74.2	35.4	18.1
HDDA	1.01	9.0	34.4	50.3	16.3	-0.4

Soft Matter Accepted Manuscript

FIG. 2: Mechanism to generate oil-coated bubbles.

4. Bubbles with Solidified Oil Coatings

In order to observe the coated-bubble morphology directly, we solidified bubble coatings of the photopolymerizable oil HDDA with 1.0 % (w.t.) photo-initiator. The polymerization proceeded fast enough (∼10 s) under UV irradiation to convert the rising oil-coated bubbles into hollow solid capsules by the time they reached the top of the column filled with a slightly viscous aqueous solution of the thickener xanthan gum. These hollow solid capsules were then collected and inspected optically.

5. Analytical Method

Bubble images (800 × 600 pixels) were taken at a speed of 500 frames per second. The terminal rising velocity was determined when velocity reached a plateau value. This was usually achieved within 0.5 s and within the first 15 cm above the bottom of the column.

As shown in Figure 3, we used Image J software to analyze the shape of the bubbles. The aspect ratio is defined as the minor axis, b, over major axis, a, which is in the range of 0 to 1. A higher aspect ratio indicates a more spherical bubble. We set 0.9 as an operational threshold for delineating a spherical shape.

B. Numerical Method

The incompressible continuity and Navier-Stokes equations have been solved in the volume-of-fluid framework for numerically simulating a rising bubble in a quiescent liquid. The governing equations are as follows:

$$\nabla \cdot \mathbf{u} = 0, \tag{1}$$

$$\rho \left[\frac{\partial \mathbf{u}}{\partial t} + \mathbf{u} \cdot \nabla \mathbf{u} \right] = -\nabla p + \nabla \cdot \left[\mu(\nabla \mathbf{u} + \nabla \mathbf{u}^T) \right] + \delta \gamma \kappa \mathbf{n} - \rho g \mathbf{j}, \tag{2}$$

$$\frac{\partial c}{\partial t} + \mathbf{u} \cdot \nabla c = 0, \tag{3}$$

where $\mathbf{u} = (u, v, w)$ denotes the velocity field, with the components u, v and w in the x, y and z directions, respectively, p denotes the pressure field, ρ denotes density, μ denotes viscosity, t denotes time, g denotes the acceleration due to gravity, $\mathbf{j}$ denotes the unit vector along the vertical direction, γ denotes the interfacial tension, δ denotes the Dirac delta function (given by $|\nabla c|$), $\kappa = \nabla \cdot \mathbf{n}$ denotes the interfacial curvature and $\mathbf{n}$ denotes the outward-pointing unit

5
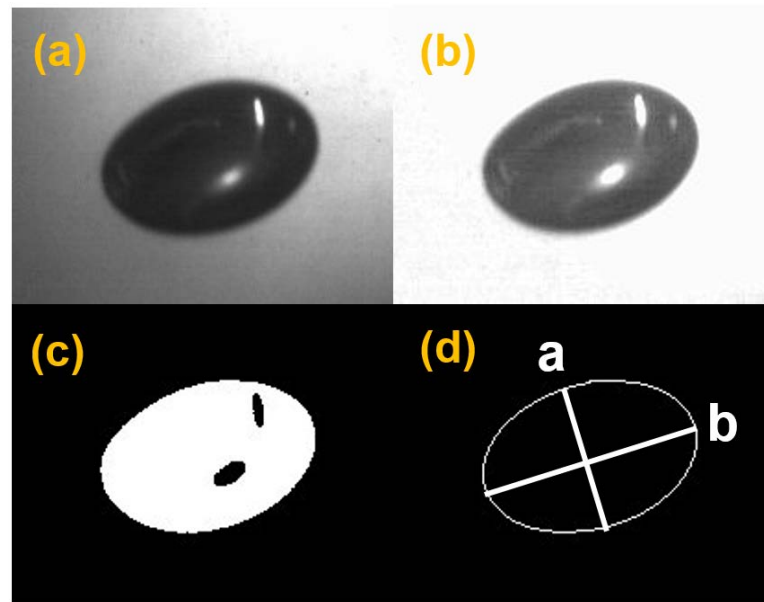
FIG. 3: Steps followed in the image processing: (a) Substract the background, (b) convert into a binary image, (c) capture the boundary of the bubbles and (d) calculate the aspect ratio.

normal to the interface. The volume fraction variable c (= 1 and 0 in the inner and outer phases, respectively) is maintained sharp by reconstructing the interface at every time step and by following a geometrical advection method [38] instead of a simple finite difference solution of the advection equation. The composite bubbles with an oil coat have been simulated in a simplified model as homogeneous *effective* bubbles with only one interface, assigned an interfacial tension corresponding to the sum of the actual oil-air and oil-water interfacial tensions, with a density given by the volume average of the air and oil density, and the viscosity of oil.

A finite volume code, Gerris [39], has been employed to solve the aforementioned equations in a Cartesian coordinate system. The domain geometry corresponds to the actual experimental setup, while the initial bubble shape has been assumed to be spherical in this numerical investigation. The present numerical code employs a balanced-force surface tension force calculation using height function based interface curvature estimation, which reduces the magnitude of spurious currents and makes the curvature estimation second order accurate. The numerical method has been tested and validated extensively in earlier works of the present authors, see for instance [31]. All data, documentation and code used in this study will be made available upon request.

III. RESULTS AND DISCUSSION

A. Bubble Morphology

The wetting behavior of the oil, air and water three-phase system can be predicted based on the spreading coefficient, $S_\circ$ [40–42], which is given by

$$S_\circ = \gamma_{aw} - \left(\gamma_{oa} + \gamma_{ow} \right), \qquad (4)$$

where subscripts aw, oa and ow denote air-water, oil-air and oil-water interfaces, respectively. The spreading coefficient can be considered as the interfacial energy benefit of replacing the air-water interface with an air-oil interface and an oil-water interface. Oils with positive spreading coefficient can spread spontaneously and form a film at the air-water interface, and thus completely engulf an air bubble in water. Oils with negative spreading coefficient, by contrast, form an oil lens at a flat air-water interface, and only partially engulf an air bubble.

Oil-air surface tension and oil-water interfacial tension were measured using the pendant drop method (ramé-hart Instrument Co.). Table I shows the measured tensions and the corresponding spreading coefficients for oils used in this work. Figure 4 shows a typical image of an air bubble and of a silicone oil coated air bubble dispensed from the orifice of the bubble generator.
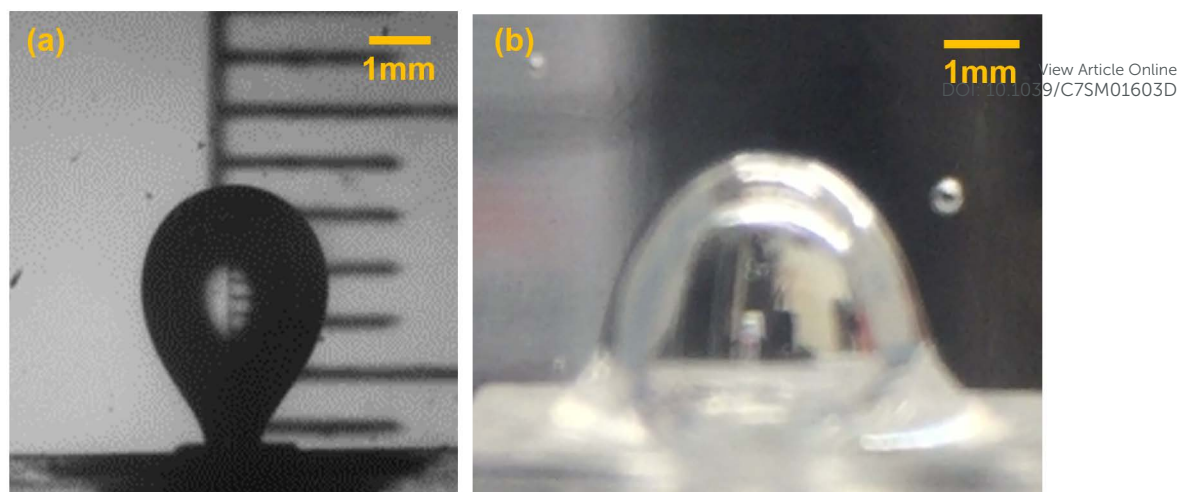
FIG. 4: Typical images of (a) standard air bubble, and (b) silicone oil coated air bubble.

While it is easy to observe the static bubble morphology, it is more challenging to image a rising bubble. The oil layer is not uniform around the whole bubble because of hydrodynamic effects, with a thinner "front end" and a thicker "rear end". The varying thickness of the oil layer can be difficult to estimate based on in situ photography alone (see Figure 5, a typical image of a silicone oil coated bubble rising in deionised water).
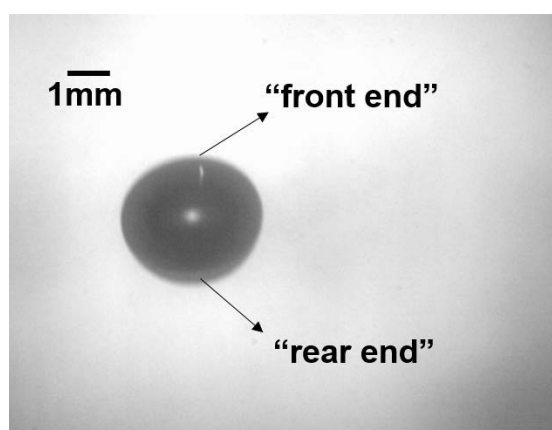

FIG. 5: Image of a silicone oil coated bubble rising in deionised water.

To further characterize the morphology of a rising coated bubble (especially the morphology at the "front end"), we used HDDA with 1.0% (w.t.) photo-initiator as the bubble coating. It also has positive spreading coefficient and can completely engulf the air bubble. It took less than 2 s for the polymerization to initiate under UV irradiation. We added xanthan gum into deionised water to increase the viscosity such that the coated-bubble can stay in the column for at least 10 s, which is enough for the polymerization to complete. Solid hollow spheres were formed before the bubbles reached to the top of the column (Figure 6). It is obvious that the oil layer is uneven around the whole bubble when it is rising. It is thinner at the "front end" than the "rear end", but the oil layer is indeed complete and continuous even at the front. It should be mentioned that the amount of HDDA used to produce the solid bubble coat shown in Figure 6 is exaggerated for experimental convenience, while all the following observations of bubble size, trajectory, velocity and shape are based on coated bubbles with a much smaller amount of oil (as shown in Figure 5). The added weight of oil was taken into account by using a volume averaged bubble density (200 kg/m^3), which was estimated based on the experimental air and oil flow rates (0.05 mL/min for the gas and 0.01 mL/min for the oil).
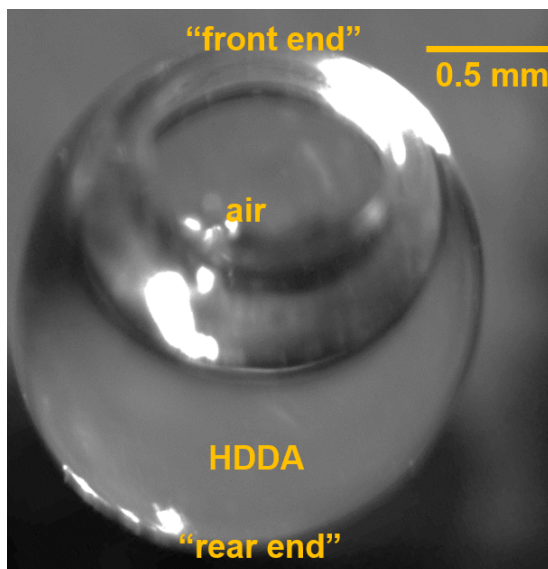
FIG. 6: Image of a HDDA-coated bubble after polymerization.

B. Bubble Size

The detachment of an air bubble at the orifice inside the water medium can be obtained by balancing the buoyancy and surface tension forces. The size of a standard bubble just prior to pinch off can be estimated as follows (Tate's law) [43]

$$(\rho_w - \rho_a)\, gV = \pi d\gamma_{aw},\qquad(5)$$

where d is the orifice diameter, V is bubble volume, and ρ_w and ρ_a are the densities of water and air, respectively. We define D as the equivalent volume spherical bubble diameter and express the bubble volume in terms of D as $V = \pi D^3/6$. Neglecting air density from Eq. (5) by assuming $\rho_a << \rho_w$, we obtain

$$\frac{D}{d} = 1.82 Bo^{-1/3},\qquad(6)$$

where

$$Bo = \frac{gd^2\rho_w}{\gamma_{aw}}\qquad(7)$$

is the so-called Bond number or Eötvös number. Eq. (6) expresses the non-dimensional bubble diameter with respect to a non-dimensional group. It is worth noting that Tate's law is based on the assumption that the bubble neck is vertical at the orifice and the surface tension force is completely downwards. However, this is typically invalid, and the exponent and coefficient need to be corrected accordingly [44]. Here we obtained an empirical correlation (Eq. (8)) by fitting our experiment results (as shown in Figure 7)

$$\frac{D}{d} = 1.65 Bo^{-0.41}.\qquad(8)$$

The discrepancy of the exponent and coefficient relative to Eq. (6) may account for the specific experiment conditions, such as the gas flow rate and the volume of the chamber below the orifice, which have been shown by Davidson *et al.* [43] to have some influence on the bubble size.

We can also extend this correlation to oil-coated bubbles, but the a/w interfacial tension needs to be replaced with an effective bubble/fluid interfacial tension to account for the joint contributions of two interfaces. This effective tension can be approximated as the sum of the air-oil and oil-water interfacial tensions (62.2 mN/m and 55.4 mN/m for silicon oil coated bubbles and octane coated bubbles, respectively), which is consistent with the simulation results in the following section.
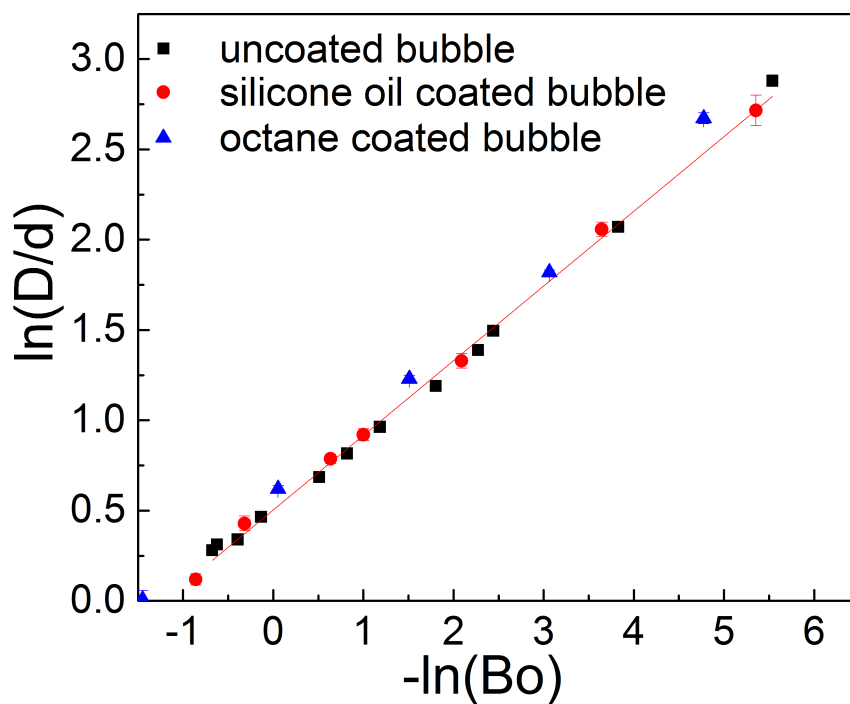
FIG. 7: Eq. (8) (line), and experimental results (symbols) for uncoated and oil-coated bubbles.
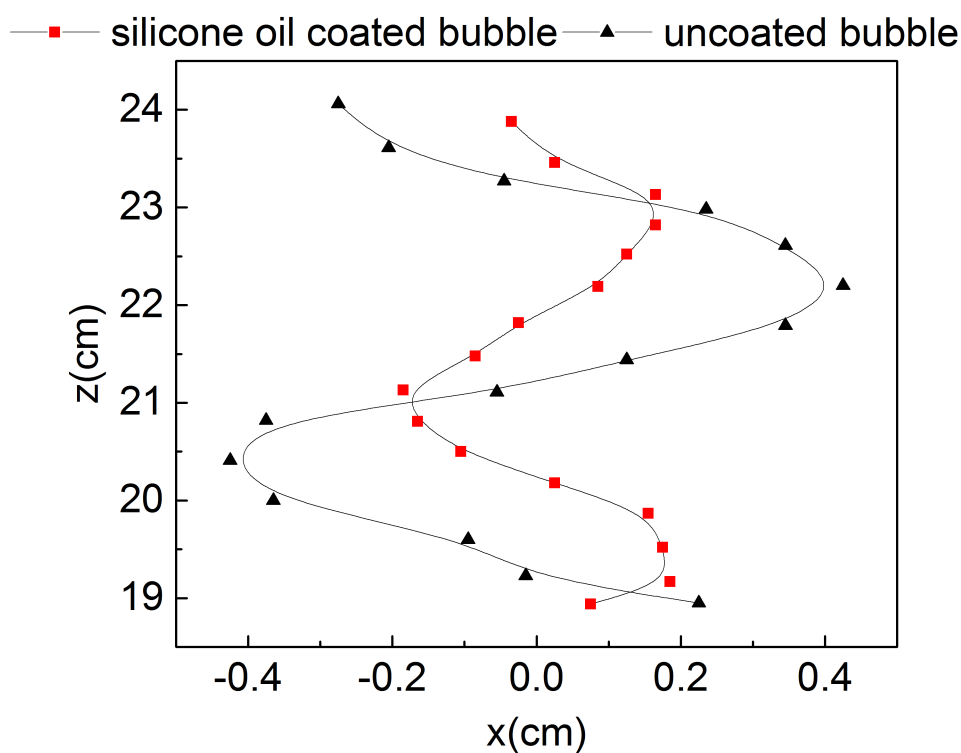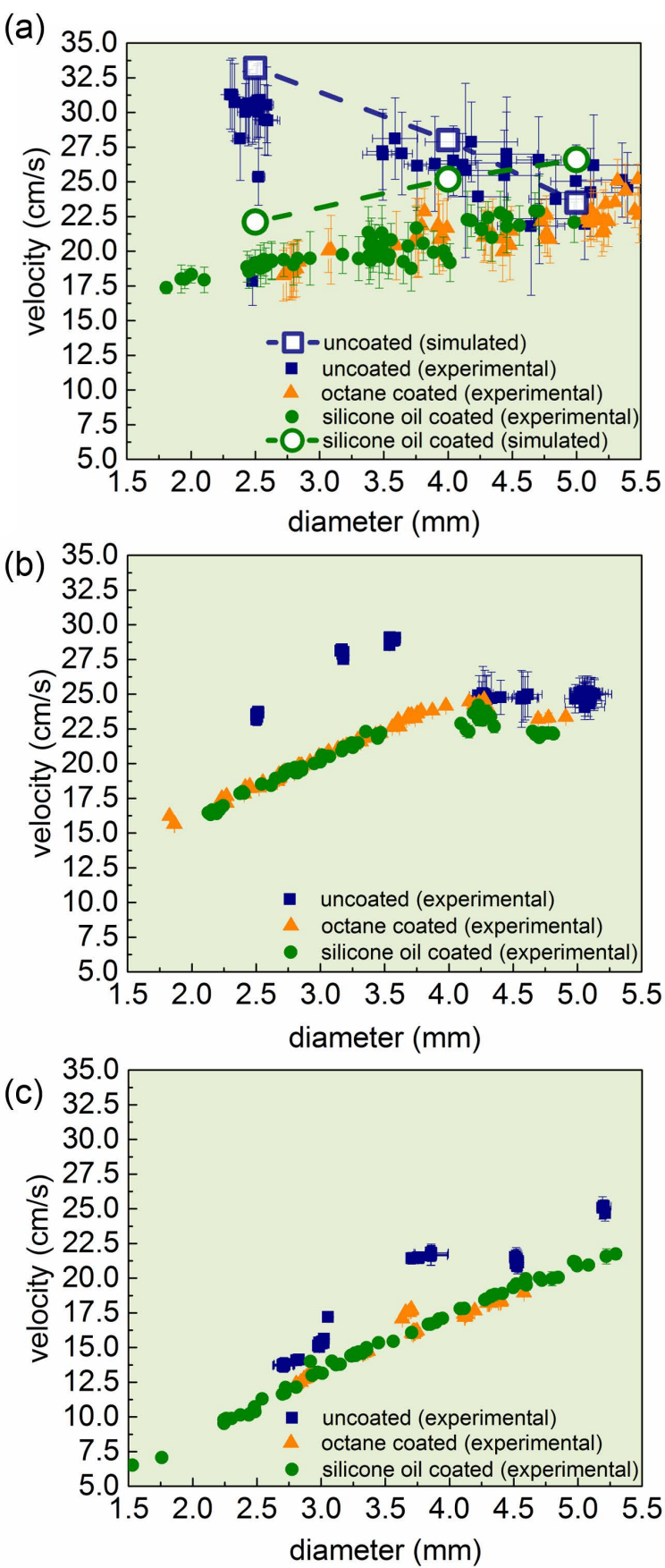

FIG. 8: Typical trajectories of uncoated and oil-coated bubbles in deionised water. Bubble diameter $D = 4$ mm.

FIG. 9: Terminal rising velocity of uncoated and oil-coated bubbles in (a) deionised water; (b) 40% (w.t.) sugar solution and (c) 50% (w.t.) sugar solution.
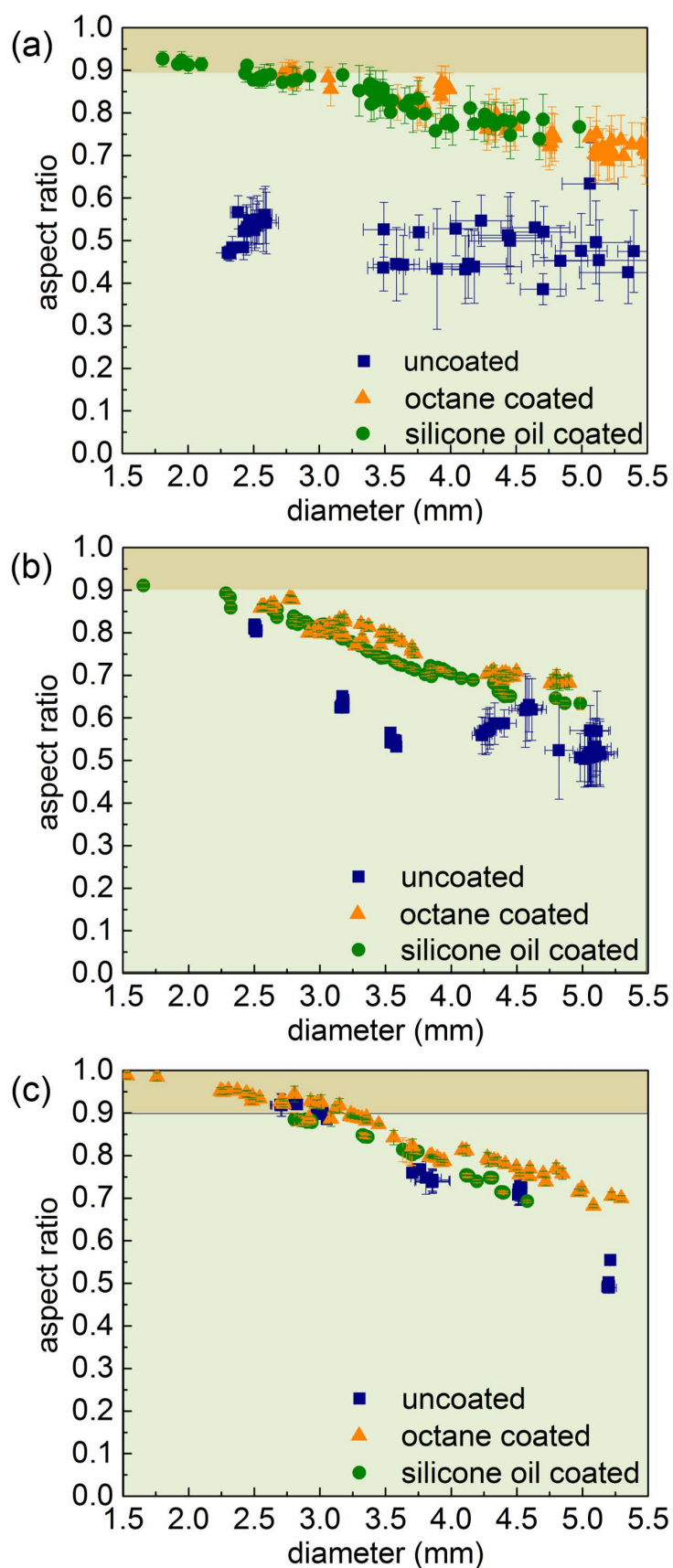
FIG. 10: Experimental aspect ratio of uncoated and oil-coated bubbles in (a) deionised water; (b) 40% (w.t.) sugar solution and (c) 50% (w.t.) sugar solution.

As Figure 7 shows, Eq. (8) is in excellent agreement with experimental data for uncoated bubbles and oil-coated bubbles alike. We see that a model description for the bubble size dependence of uncoated bubbles on surface tension can also be applied to the oil-coated bubbles, provided that the surface tension is replaced by an appropriately chosen effective tension. Given how much more is known about uncoated bubbles than about coated bubbles, one might hope that equivalent behavior can be established more generally between coated bubbles and uncoated bubbles with appropriately chosen effective values for their governing properties.

C. Bubble Rising Trajectory

Typical trajectories of uncoated and silicone oil coated bubble of comparable size are shown in Figure 8. Both bubbles exhibit zigzagging trajectories when rising in water, but oil-coated bubbles display lateral excursions of lower amplitude.

D. Bubble Rise Velocity

We measured the terminal rise velocity versus overall bubble diameter for both uncoated and oil-coated bubbles in three different fluids, namely, pure water (Figure 9a), 40% (w.t.) sugar solution (Figure 9b) and 50% (w.t.) sugar solution (Figure 9c). In all cases, oil-coated bubbles display lower rise velocity than uncoated bubbles. Lower velocity implies increased residence time for bubbles in a slurry during froth flotation and a consequently longer particle-bubble interaction time, likely to benefit flotation performance. Beyond this, Figure 9 is consistent with a well-known trend[45] that the bubble rise velocity increases with bubble size up to some threshold size, but decreases for larger bubbles when shape oscillations become more pronounced. The lower rise velocity of oil-coated bubbles can be attributed to the reduced buoyant force caused by smaller density mismatch between the bubble and the aqueous phase, as shown in the following simulation results.

E. Bubble Shape

We plot the aspect ratio versus bubble diameter rising in deionised water, 40% (w.t.) sugar solution and 50% (w.t.) sugar solution for both uncoated and oil-coated bubbles in Figure 10(a), (b) and (c), respectively. 0.9 is often set as the threshold for a spherical shape. As we can see, oil-coated bubbles always display a more spherical shape than the uncoated bubbles. The suppression of shape oscillations by the oil coat also allows for a more precise measurement of the bubble size (smaller error bars). As simulation results shown below suggest, both the added weight of the oil and the effective increase in bubble viscosity contribute to keeping the oily bubbles more spherical.

It is interesting to note that oil-coated bubbles rising in clean fluids show similarities with uncoated bubbles rising in surfactant-contaminated fluids. Both of them display a lower rising velocity, a more spherical shape and a more stable trajectory than uncoated bubbles rising in clean fluids. The latter case has been explained by the fact that when surfactant adsorbs onto the bubble surface, it will be swept to and accumulate at the back of bubble, which decreases the local surface tension and leads to a fore-to-aft surface tension gradient [46–49]. Due to the Marangoni effect, a tangential stress appears on the bubble surface and results the reduction of bubble rise velocity. The accumulated surfactant at the rear end of the bubble forms the so-called rear stagnant cap that resists shape deformation, which is similar to the oil-mediated rigidification of the rising bubbles by an oil layer observed here.

F. Simulation Results

As mentioned obove, oil-coated bubbles in water have been treated in the simulations as a single fluid phase with a bubble of density equal to the volume average of the air and oil density, a viscosity equal to that of the oil, and an interfacial tension equal to the sum of the oil-water and air-oil interfacial tensions. Using the sum of both interfacial tensions as the effective interfacial tension is a reasonable choice to account for the joint contributions of both interfaces. The overall bubble density is estimated based on the flow rate ratio between air and oil, and its effect on the bubble behavior is shown in Figure 11, 12 and Table II. It is clear that with increased bubble density, the oil-coated bubble displays slower rise velocity and a more spherical and more stable shape. For the effective bubble viscosity, a similar sensitivity analysis is conducted: the bubble viscosity is varied from air viscosity to oil viscosity (with all other parameters fixed), and it is observed that the case with oil viscosity gives the best agreement with

experimental results (as shown in Figure 13, 14 and Table III). The increase of bubble viscosity effectively suppresses bubble shape deformation but does not change the bubble rise velocity significantly.
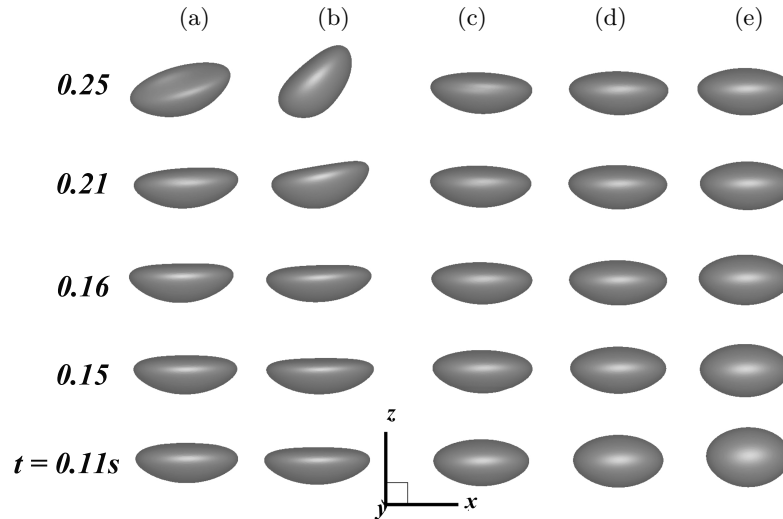

FIG. 11: Effect of the density of the inner fluid on the bubble shapes: (a) 100 kg/m^3, (b) 200 kg/m^3, (c) 300 kg/m^3, (d) 400 kg/m^3 and (e) 500 kg/m^3. The values of viscosity of the inner and outer fluids are kept equal and constant ($\mu_i = \mu_o = 1$ cP). The initial diameter of the bubble in all these cases is 4 mm.
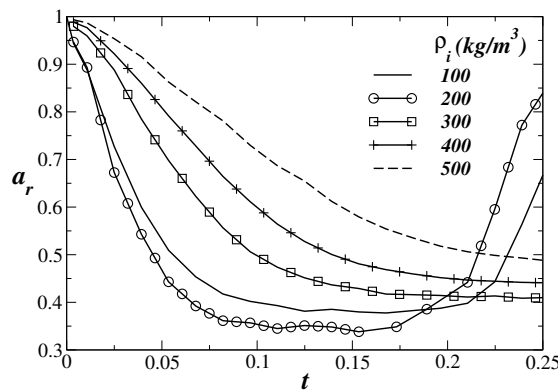

FIG. 12: Temporal variations of aspect ratios of the bubble for different values of inner fluid density. The rest of the parameters are the same as those used to generate Fig. 11.

TABLE II: Average terminal velocities for bubbles with different values of inner fluid density. The rest of the parameters are the same as those of Fig. 11.

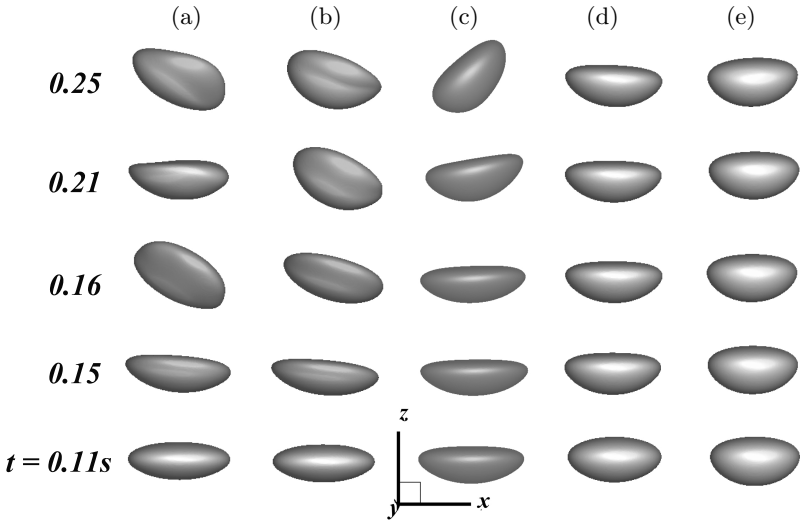| ρ_i $(\mathrm{kg \cdot m^{-3}})$	Average V_T (cm/s)
100	28.2
200	25.2
300	24.2
400	23.1
500	22.7

FIG. 13: Effect of the viscosity of the inner fluid on the bubble shapes: (a) 0.015 cP, (b) 0.15 cP, (c) 1 cP, (d) 5 cP and (e) 9.3 cP. The density of the inner and outer fluids are 200 kg/m^3 and 998 kg/m^3. The initial diameter of the bubble in all these cases is 4 mm.
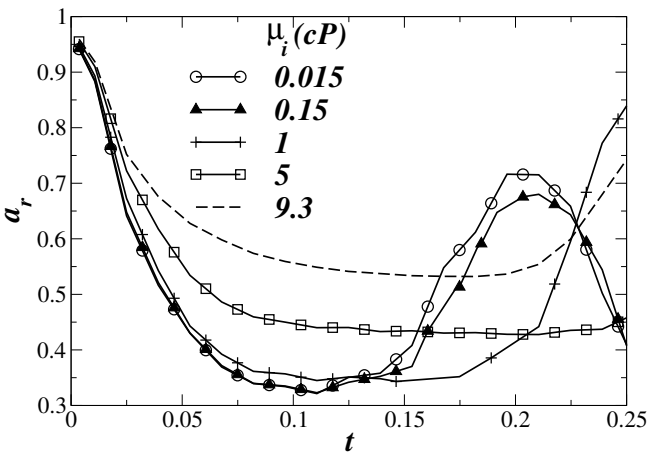

FIG. 14: Temporal variations of aspect ratios of the bubble for different values of inner fluid viscosity. The rest of the parameters are the same as those used to generate Fig. 13.

TABLE III: Average terminal velocities for bubbles with different values of inner fluid viscosity. The rest of the parameters are the same as those of Fig. 13.

μ_i (cP)	Average V_T (cm/s)
0.015	25.2
0.15	25.3
1	25.2
5	25.3
9.3	25.0

Based on the notion that the bubble buoyancy should be determined by the volume average density of their air and oil portion, considering further that the interfacial tensions of the air-oil and oil-water interface should be added to estimate their combined effect, and accounting for the observed viscosity effect on bubble shape and velocity, appropriate simulation parameters are assigned to enable direct comparison between the coated and uncoated bubbles of comparable size. For silicone oil-coated bubbles, effective bubble density, viscosity and interfacial tension are set to 200 kg/m^3, 9.3 cP and 63 mN/m, respectively. Figure 15 and 16 show the path (Figure 15) and the shape (Figure 16) of rising bubbles of $D = 2.5$ mm, 4 mm and 5 mm respectively, as obtained from the numerical simulations. The bubble shape is observed to ossicilate more with increasing bubble size, but in all cases the shape of the "coated bubbles" is more spherical and fluctuates less than the shape of the corresponding uncoated bubble. A quantitative comparison of the aspect ratio was not possible here, because the bubble undergoes continuous shape oscillations and does not reach a "steady state", even when it has reached the terminal rise velocity. The number of shape fluctuations observed within the limited time window accessible to our simulation was insufficient to compute a meaningful aspect ratio average.

The bubble rise velocity, however, attains a steady state in a very short time period (less than 0.1 s), and the terminal velocity is determined from the final slope in Figure 17. It is instructive to compare this simulated rise velocity to the one observed experimentally. For the uncoated bubbles rising in pure water (Figure 18 and 19), the simulation results agree with the corresponding experimental results both qualitatively and quantitatively within the experimental uncertainty (Table IV and Figure 9a), except for a small difference at lowest bubble size. The result is consistent with the well-known trend[45] that the rise velocity increases with bubble size up to some threshold size, but decreases for larger bubbles when shape deformation and oscillation become more pronounced. For the simulated "silicone oil coated bubbles", Figure 9a shows qualitative agreement with experimental results that the velocity increases monotonically with bubble size, and even the slope of this increase is captured well by the simulation. However, the simulation is seen to systematically overestimate the rise velocity of "coated bubbles". This quantitative disagreement cannot be explained by an uncertainty in the bubble density, as can be seen from Table II: even simulated bubbles with much higher density than we can reasonably assume for the oil-coated bubbles in our experiments, still have higher velocities than were observed experimentally. Similarly, the discrepancy does not come from misjudging the effective viscosity: as Table III clearly shows, the simulated velocity is extremely insensitive to bubble viscosity. We attribute the quantitative difference between the measured and simulated rise velocities of the oily bubbles (Figure 9a) to the crude single-phase representation of these bubbles in our simulation, which neglects the bubbles actual composite structure and does not consider the flow recirculation within the thin film. Despite this oversimplification, the simulation is seen to capture the qualitative differences between oil-coated and uncoated bubbles very well.

Combining the information from the sensitivity analysis for the effective bubble density and viscosity, it is clear that the reduced rise velocity of oil-coated bubbles can be attributed primarily to the reduced buoyant force due to added weight of oil coat, whereas the more spherical shape and more stable trajectory appear to be caused by both buoyancy and viscosity effects of the oil. Potentially relevant details of the composite bubble morphology and of flow inside the oil coat obviously cannot be resolved in the present simplified simulations. Much more work in future

TABLE IV: Comparison of experiment (Fig. 9) and simulation (Figs. 15 and 16) with regard to the average terminal bubble velocities.

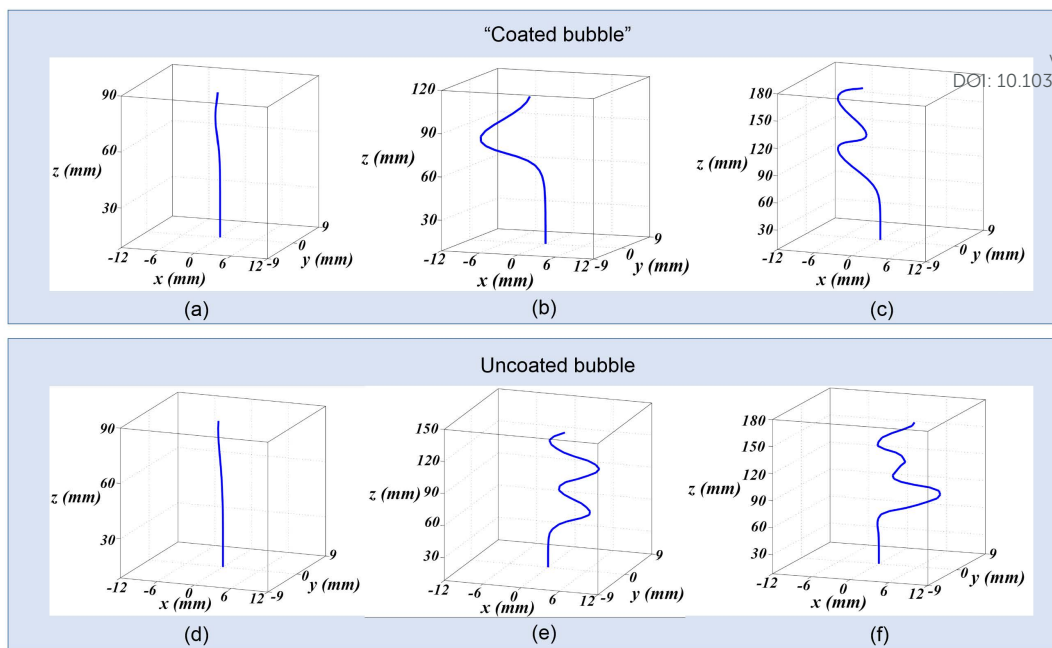| Diameter D (mm)	"Coated" (simulation) V_T (cm/s)	Coated (experiment) V_T (cm/s)	Uncoated (simulation) V_T (cm/s)	Uncoated (experiment) V_T (cm/s)
2.5	22.1	18.5 ± 1.2	33.2	30.0 ± 2.0
4	25.2	19.2 ± 1.4	28.0	26.5 ± 2.5
5	26.6	22.1 ± 1.4	23.5	22.0 ± 2.6

FIG. 15: Numerical simulation results for trajectories of a "silicone oil coated bubble" rising in water: (a) $D = 2.5$ mm, (b) $D = 4$ mm and (c) $D = 5$ mm. Numerical simulation results for trajectories of an uncoated bubble rising in water: (d) $D = 2.5$ mm, (e) $D = 4$ mm and (f) $D = 5$ mm. The quotes in the header serve as a reminder that the simulation models the coated bubbles in water as an effective two-phase system, see section II subsection B: Numerical Method.
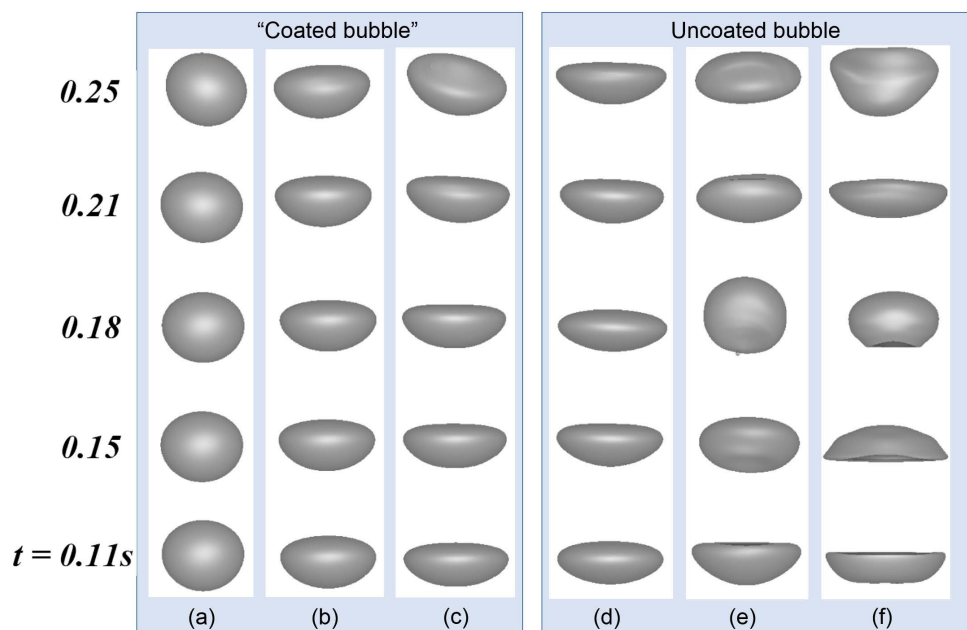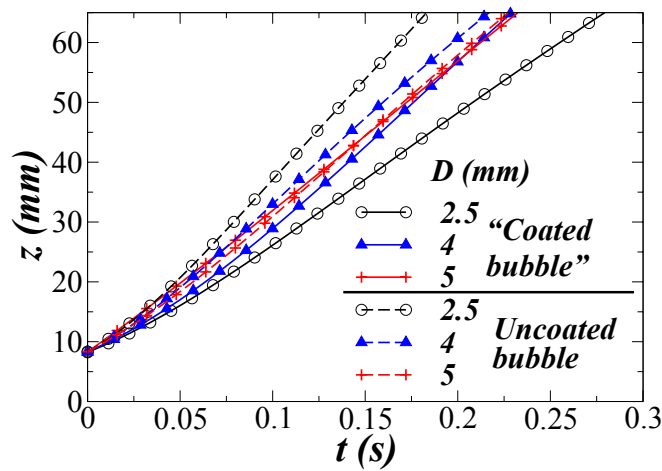

FIG. 16: Numerical simulation results for shape evolutions of a "silicone oil coated bubble" rising in water: (a) $D = 2.5$ mm, (b) $D = 4$ mm and (c) $D = 5$ mm. Numerical simulation results for trajectories of an uncoated bubble rising in water: (d) $D = 2.5$ mm, (e) $D = 4$ mm and (f) $D = 5$ mm. The quotes in the header serve as a reminder that the simulation models the coated bubbles in water as an effective two-phase system, see section II subsection B: Numerical Method.

FIG. 17: Evolution of center of gravity elevation for the bubbles shown in Figs. 15 and 16.
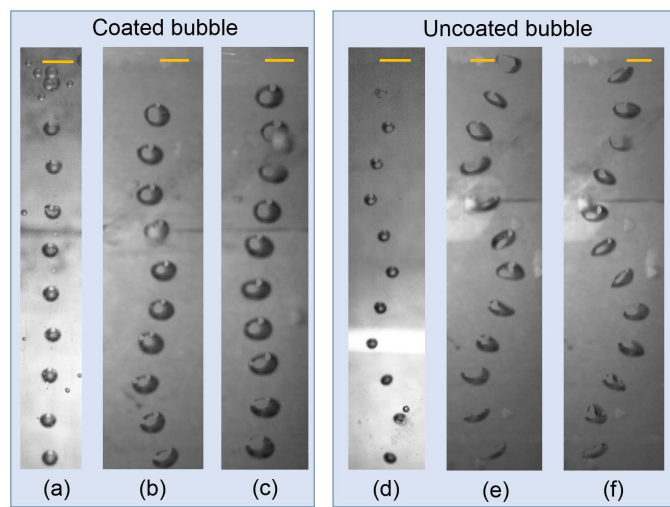

FIG. 18: Experimental results for trajectories of a silicone oil coated bubble rising in water: (a) $D = 2.5$ mm, (b) $D = 4$ mm and (c) $D = 5$ mm. Experimental results for trajectories of an uncoated bubble rising in water: (d) $D = 2.5$ mm, (e) $D = 4$ mm and (f) $D = 5$ mm. The time interval is 0.03 s and the scale bar is 5 mm.

studies will be required to remove these remaining limitations.

IV. CONCLUSIONS

In summary, the rise dynamics of a single oil-coated bubble has been systematically investigated for the first time to the best of our knowledge. The bubble morphology, size, velocity, shape and trajectory are obtained from the frames taken by the high speed camera. Oil-coated bubbles display a lower rise velocity, a steadier and more spherical shape, and less pronounced lateral excursion than uncoated bubbles of comparable size.

The experiments were complemented by bubble rise simulations based on the volume-of-fluid (VOF) method with dynamic adaptive grid refinement. Oil-coated bubbles were simulated in a simplified model as a single fluid phase with 1) an effective surface tension given by the sum of the air-oil and oil-water interfacial tensions; 2) an effective bubble density accounting for the mass contribution of oil coat, and 3) an effective bubble viscosity equal to the oil phase viscosity. Despite the simplicity of this model, the simulations captured the salient qualitative features distinguishing oil-coated and uncoated bubbles with respect to terminal velocity, bubble trajectory and bubble shape dynamics.
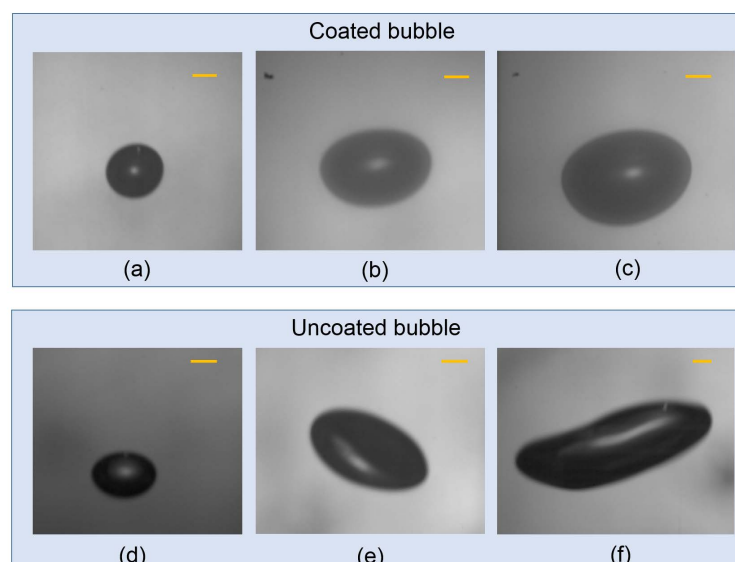
FIG. 19: Typical images of a silicone oil coated bubble rising in water: (a) $D = 2.5$ mm, (b) $D = 4$ mm and (c) $D = 5$ mm. Typical images of an uncoated bubble rising in water: (d) $D = 2.5$ mm, (e) $D = 4$ mm and (f) $D = 5$ mm. The scale bar is 1 mm.
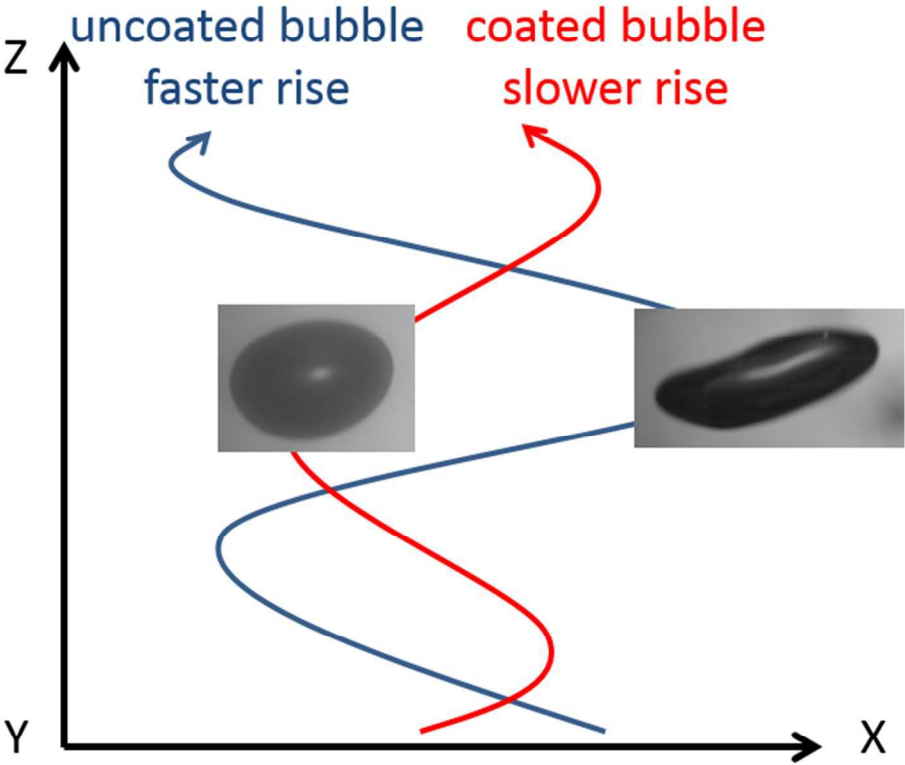
V. ACKNOWLEDGEMENTS

VI. REFERENCES

[1] Rodrigues, R. T. & Rubio, J. DAF–dissolved air flotation: Potential applications in the mining and mineral processing industry. *Int. J. Miner. Process.* **82**, 1–13 (2007).
[2] Lee, K., Archibald, D., McLean, J. & Reuter, M. Flotation of mixed copper oxide and sulphide minerals with xanthate and hydroxamate collectors. *Miner. Eng.* **22**, 395–401 (2009).
[3] Irannajad, M., Ejtemaei, M. & Gharabaghi, M. The effect of reagents on selective flotation of smithsonite–calcite–quartz. *Miner. Eng.* **22**, 766–771 (2009).
[4] Li, H., Chow, R., Roberge, K. *et al.* Role of carrier flotation in accelerating bitumen extraction recovery from mineable athabasca oil sands. *Can. J. Chem. Eng.* **91**, 1340–1348 (2013).
[5] Al-Otoom, A., Allawzi, M., Al-Omari, N. & Al-Hsienat, E. Bitumen recovery from jordanian oil sand by froth flotation using petroleum cycles oil cuts. *Energy* **35**, 4217–4225 (2010).
[6] Zhou, Z., Kasongo, T., Xu, Z. & Masliyah, J. Assessment of bitumen recovery from the athabasca oil sands using a laboratory denver flotation cell. *Can. J. Chem. Eng.* **82**, 696–703 (2004).
[7] Gübitz, G., Mansfield, S., Böhm, D. & Saddler, J. Effect of endoglucanases and hemicellulases in magnetic and flotation deinking of xerographic and laser-printed papers. *J. Biotechnol.* **65**, 209–215 (1998).
[8] Pesman, E., Imamoglu, S., Kalyoncu, E. E. & Kirci, H. The effects of sodium percarbonate and perborate usage on pulping and flotation deinking instead of hydrogen peroxide. *BioResources* **9**, 523–536 (2014).
[9] İmamoğlu, S., Karademir, A., Peşman, E., Aydemir, C. & Atik, C. Effects of flotation deinking on the removal of main colors of oil-based inks from uncoated and coated office papers. *BioResources* **8**, 45–58 (2012).
[10] Mahmoud, M. R., Lazaridis, N. K. & Matis, K. A. Study of flotation conditions for cadmium (ii) removal from aqueous solutions. *Process Saf. Environ.* **94**, 203–211 (2015).
[11] Fu, F. & Wang, Q. Removal of heavy metal ions from wastewaters: A review. *J. Environ. Manage.* **92**, 407–418 (2011).
[12] Rubio, J., Souza, M. & Smith, R. Overview of flotation as a wastewater treatment technique. *Miner. Eng.* **15**, 139–155 (2002).

[13] Sis, H. & Chander, S. Reagents used in the flotation of phosphate ores: A critical review. *Miner. Eng.* **16**, 577–585 (2003).

[14] Fuerstenau, M. C., Jameson, G. J. & Yoon, R.-H. *Froth flotation: A century of innovation* (SME, 2007).

[15] Liu, J., Mak, T., Zhou, Z. & Xu, Z. Fundamental study of reactive oily-bubble flotation. *Miner. Eng.* **15**, 667–676 (2002).

[16] Taggart, A. F. *Handbook of ore dressing* (J. Wiley & sons, Incorporated, 1927).

[17] Zhou, F. *et al.* Application of reactive oily bubbles to bastnaesite flotation. *Miner. Eng.* **64**, 139–145 (2014).

[18] Zhou, F., Wang, L., Xu, Z., Liu, Q. & Chi, R. Interaction of reactive oily bubble in flotation of bastnaesite. *J. Rare Earth.* **32**, 772–778 (2014).

[19] Zhou, F., Wang, L., Xu, Z., Liu, Q. & Chi, R. Reactive oily bubble technology for flotation of apatite, dolomite and quartz. *Int. J. Miner. Process.* **134**, 74–81 (2015).

[20] Wallwork, V., Xu, Z. & Masliyah, J. Bitumen recovery with oily air bubbles. *Can. J. Chem. Eng.* **81**, 993–997 (2003).

[21] Su, L., Xu, Z. & Masliyah, J. Role of oily bubbles in enhancing bitumen flotation. *Miner. Eng.* **19**, 641–650 (2006).

[22] Chen, F., Finch, J., Distin, P. & Gomez, C. Air assisted solvent extraction. *Can. Metall. Q.* **42**, 277–280 (2003).

[23] Tarkan, H. & Finch, J. Air-assisted solvent extraction: Towards a novel extraction process. *Miner. Eng.* **18**, 83–88 (2005).

[24] Maiolo, J. & Pelton, R. Aerosol-enhanced flotation: A possible approach to improved flotation deinking. *J. Pulp Pap. Sci.* **24**, 324–328 (1998).

[25] Gomez, C., Acuna, C., Finch, J. & Pelton, R. Aerosol-enhanced flotation deinking of recycled paper: Silicone oil offers an effective way of forming a layer on the bubble surface. *Pulp Pap. Canada* **102**, 28–30 (2001).

[26] Clift, R., Grace, J. & Weber, M. *Bubbles, drops and particles* (Dover Publications, Inc, New York, 1978).

[27] Sussman, M. & Puckett, E. G. A coupled level set and volume-of-fluid method for computing 3D and axisymmetric incompressible two-phase flows. *J. Comput. Phys.* **162**, 301–337 (2000).

[28] Magnaudet, J. & Mougin, G. Wake instability of a fixed spheroidal bubble. *J. Fluid Mech.* **572**, 311–337 (2007).

[29] Cano-Lozano, J. C., Mart´inez-Bazán, C., Magnaudet, J. & Tchoufag, J. Paths and wakes of deformable nearly spheroidal rising bubbles close to the transition to path instability. *Phys. Rev. Fluids* **1**, 053604 (2016).

[30] Zenit, R. & Magnaudet, J. Path instability of rising spheroidal air bubbles: A shape-controlled process. *Phys. Fluids* **20**, 061702 (2008).

[31] Tripathi, M. K., Sahu, K. C. & Govindarajan, R. Dynamics of an initially spherical bubble rising in quiescent liquid. *Nat. Commun.* **6**, 6268 (2015).

[32] Sahu, K. C. Double-diffusive instability in core–annular pipe flow. *J. Fluid Mech.* **789**, 830–855 (2016).

[33] Premlata, A., Tripathi, M. K. & Sahu, K. C. Dynamics of rising bubble inside a viscosity-stratified medium. *Phys. Fluids* **27**, 072105 (2015).

[34] Premlata, A. R., Tripathi, M. K., Karri, B. & Sahu, K. C. Dynamics of an air bubble rising in a non-Newtonian liquid in the axisymmetric regime. *J. Non-Newtonian Fluid Mech.* **239**, 53–61 (2017).

[35] Lindfors, K. Surface tension of sugar factory products. *Ind. Eng. Chem.* **16**, 813–816 (1924).

[36] Vázquez, G., Alvarez, E. & Navaza, J. M. Density, viscosity, and surface tension of sodium carbonate + sodium bicarbonate buffer solutions in the presence of glycerine, glucose, and sucrose from 25 to 40°c. *J. Chem. Eng. Data* **43**, 128–132 (1998).

[37] Zhang, Y., Wu, J., Wang, H., Meredith, J. C. & Behrens, S. H. Stabilization of liquid foams through the synergistic action of particles and an immiscible liquid. *Angew. Chem. Int. Ed.* **53**, 13385–13389 (2014).

[38] Popinet, S. An accurate adaptive solver for surface-tension-driven interfacial flows. *J. Comput. Phys.* **228**, 5838–5866 (2009).

[39] Popinet, S. Gerris: a tree-based adaptive solver for the incompressible euler equations in complex geometries. *J. Comput. Phys.* **190**, 572–600 (2003).

[40] Torza, S. & Mason, S. G. Three-phase interactions in shear and electrical fields. *J. Colloid Interface Sci.* **33**, 67–83 (1970).

[41] Pannacci, N. *et al.* Equilibrium and nonequilibrium states in microfluidic double emulsions. *Phys. Rev. Lett.* **101**, 164502 (2008).

[42] Guzowski, J., Korczyk, P. M., Jakiela, S. & Garstecki, P. The structure and stability of multiple micro-droplets. *Soft Matter* **8**, 7269–7278 (2012).

[43] Davidson, L. & Amick, E. H. Formation of gas bubbles at horizontal orifices. *AIChE J.* **2**, 337–342 (1956).

[44] Benzing, R. J. & Myers, J. E. Low frequency bubble formation at horizontal circular orifices. *Ind. Eng. Chem. Res.* **47**, 2087–2090 (1955).

[45] Gaudin, A. M. *Flotation* (McGraw-Hill, 1957).

[46] Ratulowski, J. & Chang, H.-C. Marangoni effects of trace impurities on the motion of long gas bubbles in capillaries. *J. Fluid Mech.* **210**, 303–328 (1989).

[47] Cuenot, B., Magnaudet, J. & Spennato, B. The effects of slightly soluble surfactants on the flow around a spherical bubble. *J. Fluid Mech.* **339**, 25–53 (1997).

[48] Takagi, S. & Matsumoto, Y. Surfactant effects on bubble motion and bubbly flows. *Ann. Rev. Fluid Mech.* **43**, 615–636 (2011).

[49] Dukhin, S., Lotfi, M., Kovalchuk, V., Bastani, D. & Miller, R. Dynamics of rear stagnant cap formation at the surface of rising bubbles in surfactant solutions at large reynolds and marangoni numbers and for slow sorption kinetics. *Colloids Surf. A* **492**, 127–137 (2016).

122x110mm (150 x 150 DPI)